Electronic Supplementary Material (ESI) for Energy & Environmental Science. This journal is © The Royal Society of Chemistry 2021

Supporting Information

Improved performance and stability of perovskite solar modules by interface modulating with Graphene Oxide crosslinked $CsPbBr_3$ Quantum Dots

Shujing Zhang,*[a] Rui Guo,*[a] Haipeng Zeng,[a] Yang Zhao,[a] Xingyue Liu,[b] Shuai You,[a] Min Li,[a] Long Luo,[a] Monica Lira-Cantu[c], Lin Li,[a] Fengxiang Liu,[a] Xin Zheng,[a] Guanglan Liao,[b] and Xiong Li*[,a]

a. *Michael Grätzel Center for Mesoscopic Solar Cells, Wuhan Photoelectric National Research Center, Huazhong University of Science and Technology, 1037 Luoyu Road, Wuhan, 430074, P. R. China.*

b. *State Key Laboratory of Digital Manufacturing Equipment and Technology, Huazhong University of Science and Technology, Wuhan 430074, China*

Email: xiongli@hust.edu.cn

c. *Catalan Institute of Nanoscience and Nanotechnology (ICN2), CSIC and the Barcelona Institute of Science and Technology (BIST), Campus UAB, Bellaterra, Barcelona, 08193 Spain*

Experimental Section

Synthesis of QDs:

(1) Synthesis of cesium oleate. 0.0814 g of cesium carbonate (Cs_2CO_3), 4 mL of octadecene (ODE), and 0.25 mL of oleic acid (OA) were added to 50 mL 3-necked round-bottom flask by stirring under vacuum at 120 °C for 1 h to remove moisture and O_2 until the solution became transparent. (2) Synthesis of colloidal $CsPbBr_3$ QDs. ODE (5 mL), OAm (0.5 mL), OA (0.5 mL), and $PbBr_2$ (0.0524 g) were added to a 50 ml three-neck round-bottom flask, stirring and deaerating for 1 h at 120 °C. The temperature of lead precursor solution was elevated to 160 °C until the solution was no longer releasing gas under N_2 atmosphere. 0.40 mL cesium oleate was swiftly injected via syringe. After 5 s, a green mixture appeared and the flask was immediately immersed into an ice water bath. The synthesized QDs were precipitated by adding ethyl acetate. The mixture was centrifuged at 8000 rpm, 5 min. The precipitated QDs are dispersed in chloroform.

Synthesis of GO/QDs composite:

GO was dispersed in chloroform by ultrasonication for 4 h. GO/QDs composite was prepared by mixing 1 mg/ml GO suspension with QDs colloid solution (10 mg/ml) and stirred for 48 h. The resulting GO/QDs composite was purified following the same procedure as described for the synthesis of QDs.

PSCs fabrication:

The ITO substrates were cleaned by sequential sonication with detergent, deionized water, ethanol, and isopropyl alcohol (IPA) for 15 min each. SnO_2 electron transport layer (ETL) was deposited following previous work.[35] Then filtered SnO_2 colloidal solution with heparin potassium was spin-coated at 4000 rpm for 30 s, followed by annealing at 150 ℃ for 30 min. The VASP method was used to fabricate high-quality perovskite film inside a N_2-filled glovebox.[6] The perovskite precursor was prepared by mixing 245.05 mg FAI, 656.9 mg PbI_2, 8.4 mg MABr, 27.68 mg $PbBr_2$, 33 mg MACl in a mixed solvent of DMF, DMSO, and GBL with a volume ratio of 2:1:2. For each sample, the filtered solution was deposited over the substrate by two consecutive spin-coating steps of 1,000 rpm and 4,000 rpm for 28s and 18s, respectively. The wet film was put into a sealed sample chamber connected to a home-built vacuum pumping system and immediately exposed to low pressure (20 Pa) for 10 s. Subsequently, the perovskite film was put on a hotplate and annealed at 100°C for 45 min. The QDs colloid solution or GO/QDs colloid solution was spin-coated on top of annealed perovskite film at 3,000 rpm for 30 s. The hole transporting layer (HTL) was spin-coated at 3000 rpm for 30 s. For Spiro-MeOTAD layer, 72.3 mg Spiro-MeOTAD mixed 17.5 µL Li-TFSI (520 mg/mL in acetonitrile) and 28 µL tBP in 1 ml chlorobenzene solution. For P3HT solution, 15 mg/ml mixed 20.4 µL Li-TFSI and 20.4 µL tBP. Finally, an 80 nm thick gold electrode was deposited by thermal evaporation.

PSMs fabrication:

The module fabrication process was complicated. A nanosecond laser P1 was pre-patterned on ITO (6×6 cm^2) to form the patterned module substrate. The ETL, perovskite, GO/QD interlayer, and HTL were fabricated with the same process with more solvent dosage. Spiro-MeOTAD was used for HTL. After depositing the ETL, perovskite layer, GO/QD interlayer, and HTL, the P2 line was laser-scribed. At last, a gold electrode was deposited by thermal evaporation using a shadow mask to pattern the electrodes, and etched by mechanical scribing (P3) to form the series-connected module. The aperture area of the PSMs is 17.11 cm^2. For thermal

stability test, the HTL was replaced by a radical polymer of poly(4-glycidyloxy-2,2,6,6-tetramethylpiperidine-1-oxyl) modified Spiro-OMeTAD/P3HT (volume ratio 7:1) mixture.

PSM encapsulation

Module encapsulation is according to reference[1]. Polymer polyisobutylene (PIB) was used for encapsulation of the PSMs. Blanket encapsulation and edge seal were commonly used to ensure good hermetic packaging. Edge preparation steps were performed during the PSC fabrication process. First, the edges of the SnO_2 were chemically wiped by ethanol to create a 4–5 mm wide uncoated margin. Later, the wipe-clean step was repeated but by using isopropanol and DMSO mixture (20:1) before the Au evaporation step to remove the perovskite/interlayer/HTL at the edges, resulting in a 4–5 mm wide clean margin while the central region was protected by a fitted metal cover. The polymer sealant was aligned to those margins to make an edge seal and loaded to a pre-heated vacuum laminator for a two-step hot press. Finally, the samples were covered with a 1–2 mm thick cover glass using kapton tape.

Characterization

Compositional depth profiling of perovskite films was carried out using a TOF-SIMS 5 system from IONTOF and a Bi^{3+} primary ion beam. For depth profiling, a Cs^+ sputter beam was used to remove material layer by layer in interlaced mode, from a raster area of 300 × 300 μm^2. Mass spectrometry was performed on an area of 80 × 80 μm^2. AFM-IR experiments were conducted using a commercial AFM-IR setup (NanoIR3s, Bruker, CA, USA) that consists of an AFM microscope and a Quantum Cascade Laser (QCL laser) (MIRcat, Daylight Solutions Inc., CA, USA), that is tunable from 2350 to ≈ 870 cm^{-1} (from 4.25 to 11.49 µm). The repetition rate of the QCL laser is tunable to match the contact resonance frequencies of the AFM cantilever. The typical laser spot size is ≈ 50 µm at the sample. AFM-IR experiments were obtained from perovskite film washed by ethyl acetate under a N_2-purged environment at 1 atm in a custom enclosure built around the sample. *J–V* measurements were conducted with a digital source metre (Keithley 2400). Simulated AM 1.5G irradiation (100 mW/cm^2) was produced by a xenon-lamp-based solar simulator (Oriel 94023 A, Newport). The light intensity was calibrated by a standard silicon reference cell (Newport). The large-area PSCs were measured in reverse scan (from 1.2 to 0 V) with a scan rate of 100 mV s^{-1}. The PSMs (6 × 6 cm^2) were measured in reverse scan (from 7 to -0.2 V). The UV–vis spectra of perovskite film and QDs solution were measured by a UV-3600 spectrophotometer. The TEM and HRTEM measurements were performed on the Tecnai G20 F30 transport electron microscope (FEI Co.). The SEM images and energy dispersive spectrum (EDS) were acquired using Nova NanoSEM 450 scanning electron microscope (FEI Co., The Netherlands). The PL spectra were measured with a laser beam at 532 or 326 nm (Lab RAM HR 800 Raman Microscope). TRPL was measured in the transient mode with the excitation provided by a 470 nm diode laser (HORIBA). AFM measurements were conducted on Shimadzu SPM9700 (Japan) in tapping mode. The contact angle was measured via an optical video contact angle instrument (VCA Optima XE, AST). The Mott–Schottky measurements were carried out in the dark with the PGSTAT302N electrochemical workstation. The XRD analysis (PANalytical B.V. Co.) was used for the crystallinity and stability test with Cu Kα radiation (λ=1.5418 Å). Ultraviolet photoemission spectroscopy (UPS) measurements were carried out on an AXIS-ULTRA DLD-600W Ultra spectrometer (Kratos Co. Japan). The stability test was measured using a CHI1000C multichannel electrochemistry workstation (Chenhua, Co., China).

Table S1 Confirmed single-junction Perovskite Solar Modules and published journals in the past five years.

Mini-module	Year	V_{OC} (V)	J_{SC} (mA/cm²)	FF	PCE (%)	Test Centre	reference
1	2021	8.715	2.83	75.41	18.6	NREL	2
2	2021	10.83	1.70	72.0	15.3	National Institude of Metrology, China	3
3	2021	1.0845	20.63	74.3	16.63	NREL	4
4	2020	7.51	3.03	78.6	17.88	National Photovoltaic Product Quality Supervision & Inspection Center, China	5
5	2019	10.8	1.835	71.5	14.17	Newport	6
6	2018	7.50	2.72	71.0	14.5	AIST	7
7	2017	8.36	2.02	71.5	12.07	AIST	8

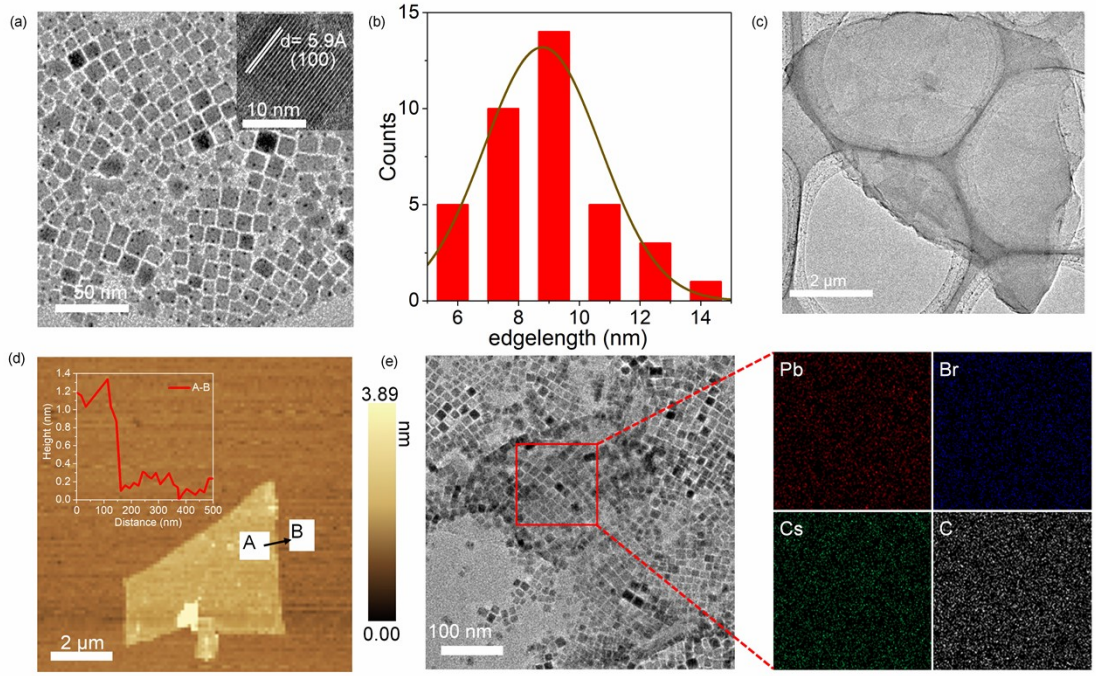

Fig. S1 (a) The TEM and HRTEM images of QDs. (b) Histogram of the size distribution of QDs. (c) The TEM of GO. (d) AFM height image of GO on SiO_2/Si. (e) The TEM of GO/QDs composite and the corresponding EDX mapping images.

From the AFM height image of GO sheet, we infer that the total thickness is 1.03 nm. This value is approximately equal to the thickness of around 1.1 nm for the single-layer GO, indicating that the solvent-exfoliated GO sheets were composed of a single layer.

The high-angle annular dark-field (HAADF) STEM image in Fig. S1e shows a uniform distribution of the cubic nanoparticles attaching on the surface of GO sheet, where the lattice fringe spacing (0.59 nm) of nanoparticles is consistent with the (100) lattice planes of $CsPbBr_3$ QDs. EDS in STEM mode confirms the presence of Cs, Pb, Br and C in the sample, and demonstrates that all these elements exhibit similar distributions. From these observations, we can conclude that the QDs are uniformly and homogeneously deposited on GO.

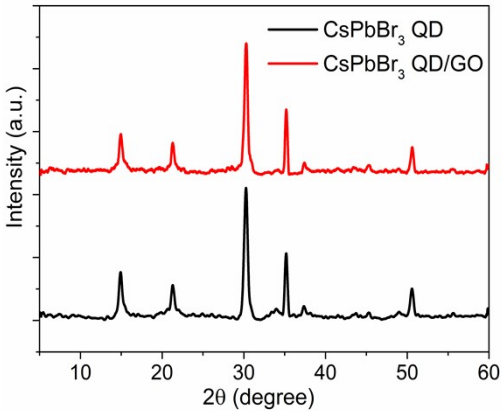

Fig. S2 Powder XRD patterns of QD_S and GO/QDs composite.

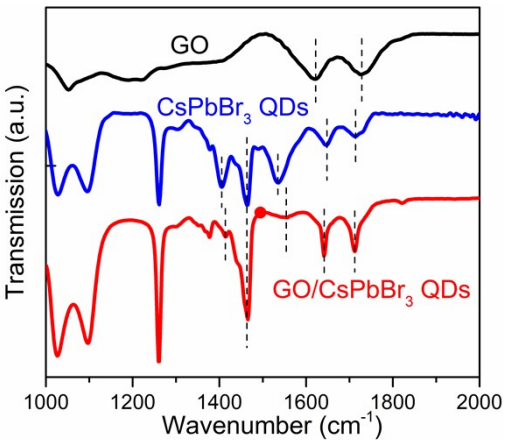

Fig. S3 FTIR spectra of the fabricated GO, QD_S, and GO/QD_S films.

For the GO, carboxyl and epoxy functional groups are detected at 1728, and 1052 cm^{-1}, respectively. The peak at 1621 cm^{-1} can be attributed to O–H bending vibrations.[9] For the QDs, peaks at 1534 and 1648 cm^{-1} are ascribed to the N–H scissor bending, and peaks at 1406, 1463, and represent the COO^- stretching vibrations, respectively.[10] For the GO/QDs composite, the C=O (1413, 1463 cm^{-1}) vibration peak and the N−H (1554, 1642 cm^{-1}) vibration peak confirmed that the insulating ligands (oleic acid and oleylamine) were retained existence in the QDs (Fig. S3). Compared with QDs, the characteristic peaks were shift which attributed to the coordination effect between the oxygen atoms of GO with the lead atoms.[11,12]

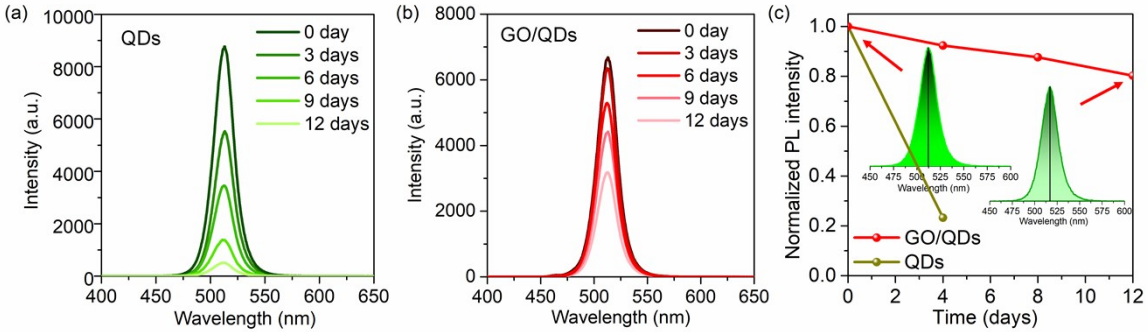

Fig. S4 Temporal evolution of PL intensities of (a) QDs and (b) GO/QDs film heated at 85 °C. (c) Relative fluorescence intensity of GO/QDs over different times aged in ambient (25 ± 5 ℃, humidity 80% ± 10%). Inset images are the PL spectrum of GO/QDs film.

The GO enhanced thermal stability of the QDs. When the QDs film was heated at 85 °C for 3 days, a sharp degradation trend was o served. The GO/QDs film kept 48% of its PL intensity while only 6% of its original PL was maintained for QDs film after heating for 12 days (Fig. S4a and b). When the GO/QDs film was exposed in air, its initial PL intensity was nearly unchanged and the sample still maintains 80% of the original PL intensity in 12 days, despite a slight red shift in PL spectra (inset Fig. S4c). In contrast, the PL intensity of QDs film was almost completely quenched after 4 days, which ascribe to the aggregation and decomposition of QDs during aging. The introduction of a barrier by crosslinking QDs with GO provides a novel strategy to afford robust perovskite QDs materials with humidity and thermal stability. These results collectively demonstrate that crosslinking interfacial modulator GO/QDs provide a permeation barrier that effectively shields the perovskite film from humidity.

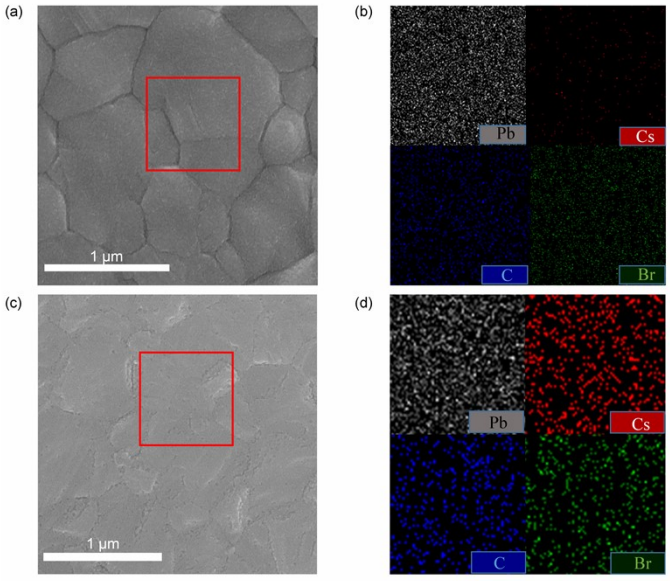

Fig. S5 Surface SEM images of perovskite: (a) pristine and (b) corresponding Pb, Cs, C, and Br elements distribution mappings in the red zone; (c) with GO/QDs interlayer and (d) corresponding Pb, Cs, C, and Br elements distribution mappings in the red zone.

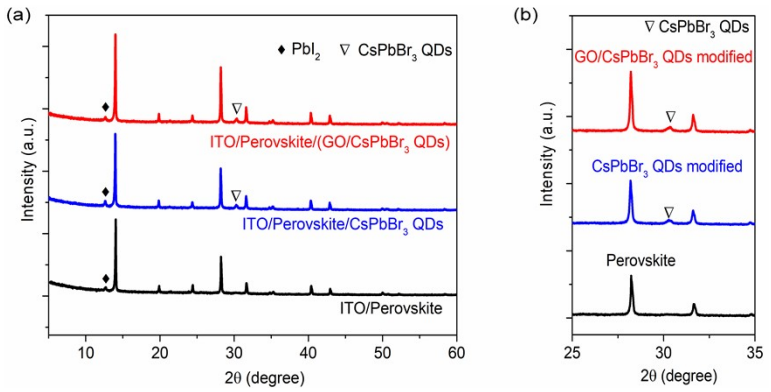

Fig. S6 (a) The XRD spectral of the perovskite film with and without modification, (b) the enlarged XRD data at 25-35°. 30.2° is characteristic peaks of $CsPbBr_3$ QD_S, correspond to (200) plane.

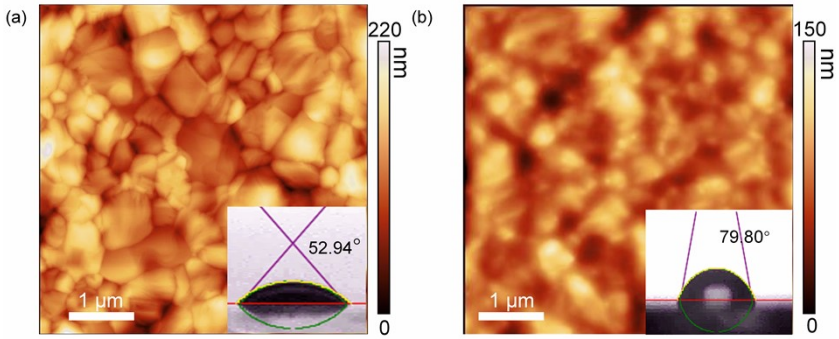

Fig. S7 AFM images of (a) pristine perovskite film and (b) perovskite film with GO/QDs interlayer. Inset: Images of water droplets.

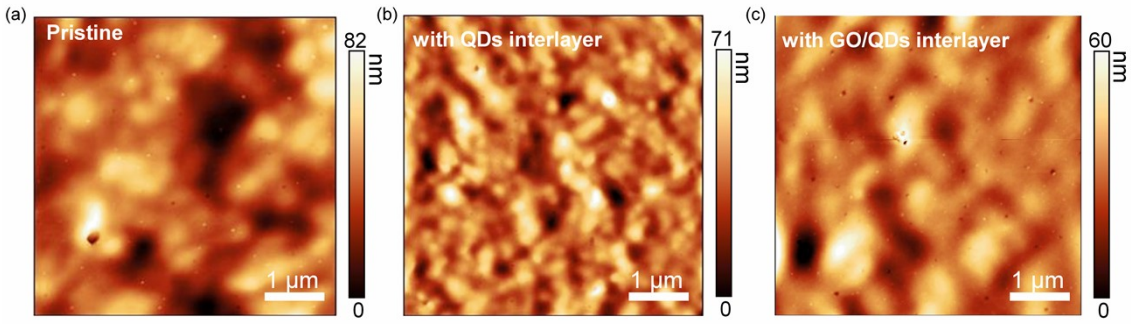

Fig. S8 AFM images of the corresponding Spiro-MeOTAD films deposited on various perovskite: (a) pristine, (b) with QDs interlayer, and (c) with GO/ QDs interlayer.

Table S2. Fitted TRPL parameters of perovskite films using two exponential fitting.

	A_1	τ_1 (ns)	A_2	τ_2 (nm)	τ_{ave} (ns)
Pristine	0.12676	68.13	0.61792	1579.35	1566.1
with QDs interlayer	0.19563	49.49	0.63534	1263.94	1249.5
with GO/QDs interlayer	0.21531	57.37	0.62513	1061.73	1043.4

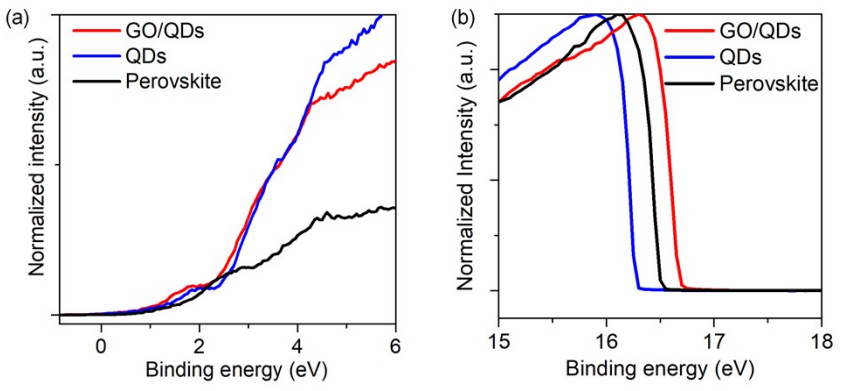

Fig. S9 The UPS data of the perovskite film, QDs film, and GO/QDs film. (a) Low-binding-energy valence band region (b) High-binding-energy cut-off region.

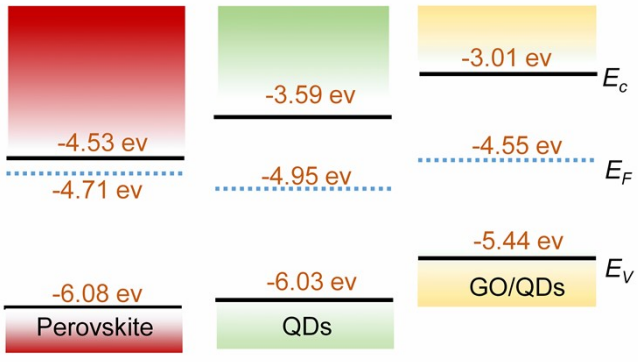

Fig. S10 Schematic energy level diagrams of perovskite layer, QDs interlayer, and GO/ QDs interlayer.

In our case, the n-type $CsPbBr_3$ QDs film showed valence band maximum (VBM) at -6.03 eV and fermi level at -4.95 eV (Fig. S10). The fermi level and VBM of p-type GO is around -4.47 eV and -5.01 eV, respectively[13] In the GO/QDs heterostructure, the fermi levels of GO and QDs has to be aligned. Therefore, the VBM of QDs layer has to bend upward.

Table S3 Detailed parameters to calculate the carrier density.

device	V_{OC} *(V)*	V_{bi} *(V)*	*Slope of* $1/C^2$ *vs.* V $(F^{-2}\ V^{-1})$	N_d (cm^{-3})
Pristine	1.08	1.05	-6.35×10^{17}	9.37×10^{11}
With QDs interlayer	1.11	1.10	-6.53×10^{17}	9.12×10^{11}
With GO/QDs interlayer	1.13	1.15	-6.92×10^{17}	8.60×10^{11}

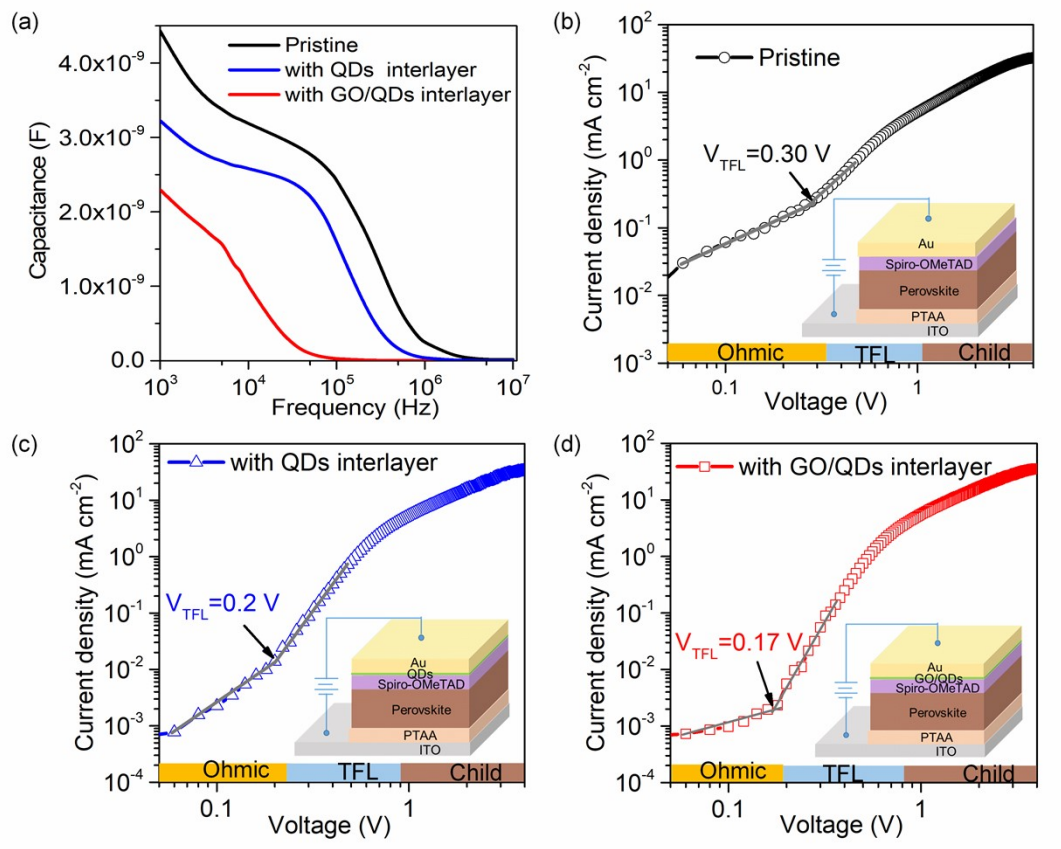

Fig. S11 (a) Capacitance–frequency plots; (b-d) dark current-voltage characteristics of the perovskite films measured using the space-charge-limited current (SCLC) method. The current density-voltage curve of hole-only devices based on different interlayers.

Table S4 The fresh and aged photovoltaic parameters of representative PSMs measured under continuous simulated AM 1.5 light illumination for 500 h.

	cell	*Voc (V)*	*Jsc (mA/cm²)*	*FF*	*PCE (%)*
Pristine	Fresh	6.21	3.70	0.69	15.87
	Aged	5.36	2.47	0.25	3.31
With QDs interlayer	Fresh	6.40	3.75	0.72	17.4
	Aged	6.30	3.27	0.63	12.98
With GO interlayer	Fresh	6.25	3.75	0.70	16.4
	Aged	6.21	3.65	0.65	14.76
With GO/QDs interlayer	Fresh	6.48	3.71	0.76	18.27
	Aged	6.51	3.68	0.72	17.25

The photovoltaic parameters of the devices were shown in Table S4. The PCE of PSC containing QDs interlayer show 9.6% improvement in PCE (from 15.87% to17.4%), whereas the PCE of PSC containing GO interlayer show

3.3% improvement in PCE (from 15.87% to 16.4%), suggesting the QDs component rather than the GO segment in GO/QDs interlayer plays the dominant effect on the photovoltaic performance improvement. The PCE of PSC containing QDs interlayer dropped 25.5% (from 17.4% to 12.98%) under illumination after 500 h, whereas the PCE of PSC with GO interlayer dropped 10% (from 16.4% to 14.76%), implying the GO segment rather than the QDs component in GO/QDs interlayer exerts a key role in long-term stability enhancement.

Table S5 The detailed parameters for the 1 cm^2 PSCs employing P3HT as HTL.

P3HT-HTL	J_{SC} (mA/cm^2)	V_{OC} (V)	*FF*	*PCE (%)*
Pristine	22.91	1.001	0.759	17.41
with QDs interlayer	22.75	1.083	0.743	18.29
with GO/QDs interlayer	23.49	1.093	0.76	19.52

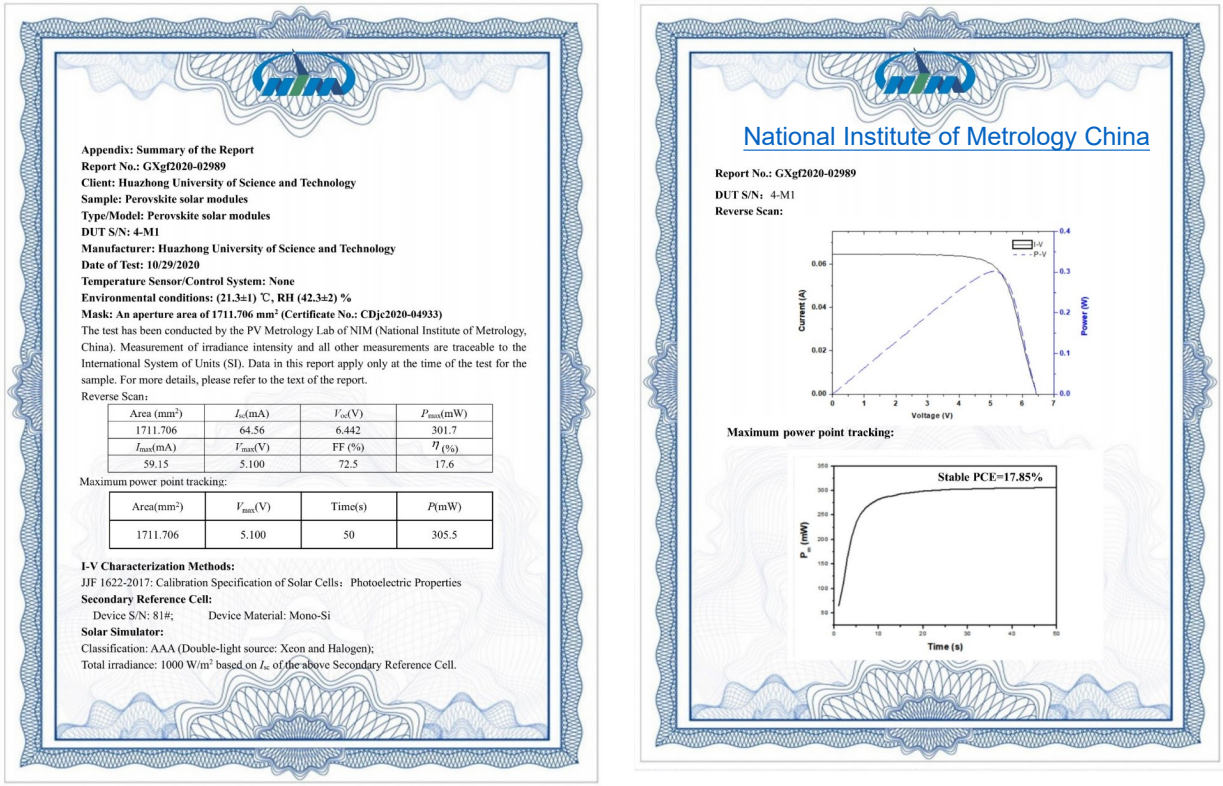

Appendix: Summary of the Report
Report No.: GXgf2020-02989
Client: Huazhong University of Science and Technology
Sample: Perovskite solar modules
Type/Model: Perovskite solar modules
DUT S/N: 4-M1
Manufacturer: Huazhong University of Science and Technology
Date of Test: 10/29/2020
Temperature Sensor/Control System: None
Environmental conditions: (21.3±1) ℃, RH (42.3±2) %
Mask: An aperture area of 1711.706 mm² (Certificate No.: CDjc2020-04933)
The test has been conducted by the PV Metrology Lab of NIM (National Institute of Metrology, China). Measurement of irradiance intensity and all other measurements are traceable to the International System of Units (SI). Data in this report apply only at the time of the test for the sample. For more details, please refer to the text of the report.
Reverse Scan:

Area (mm^2)	I_{sc}(mA)	V_{oc}(V)	P_{max}(mW)
1711.706	64.56	6.442	301.7
I_{max}(mA)	V_{max}(V)	FF (%)	η (%)
59.15	5.100	72.5	17.6

Maximum power point tracking:

Area(mm^2)	V_{max}(V)	Time(s)	P(mW)
1711.706	5.100	50	305.5

I-V Characterization Methods:
JJF 1622-2017: Calibration Specification of Solar Cells：Photoelectric Properties
Secondary Reference Cell:
Device S/N: 81#; Device Material: Mono-Si
Solar Simulator:
Classification: AAA (Double-light source: Xeon and Halogen);
Total irradiance: 1000 W/m^2 based on I_{sc} of the above Secondary Reference Cell.

Fig. S12 The performance of a perovskite solar module certified by a public test center (National Institute of Metrology, China)

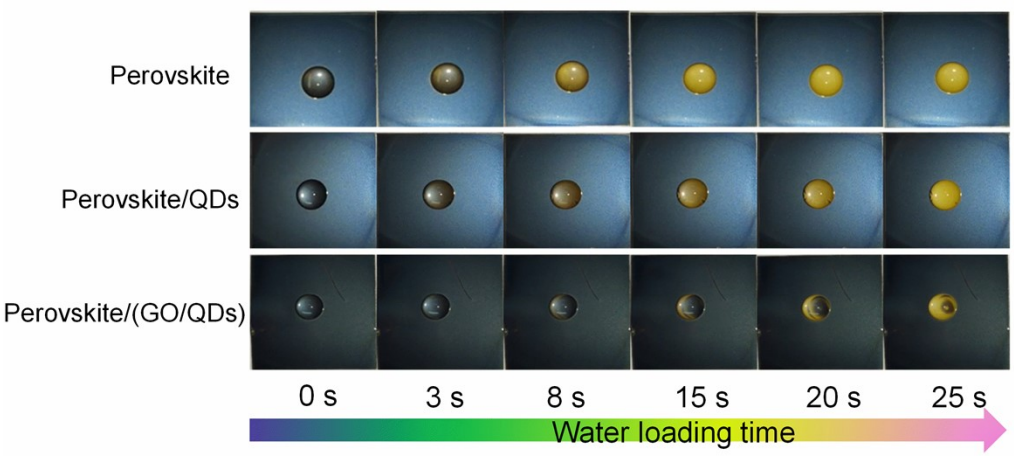

Fig. S13 The degradation images of the perovskite films with different interlayers by dropping a drop of water upon the surfaces.

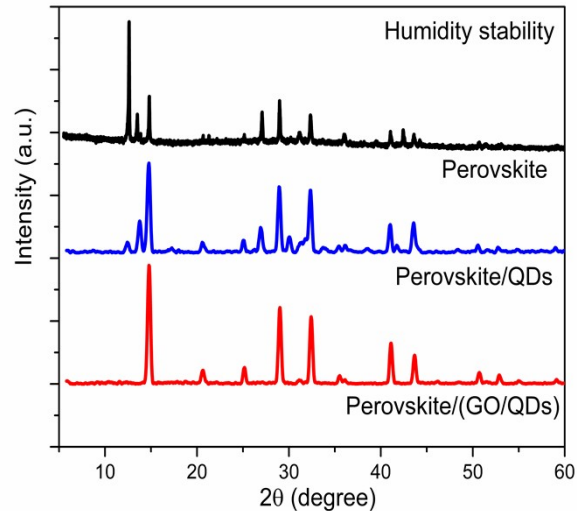

Fig. S14 X-ray diffraction (XRD) spectra for perovskite films heated at 100 ℃ in ambient air (80% RH) for 5 days. PbI_2 peak (12.8°) and δ-phase peak (11.8°)

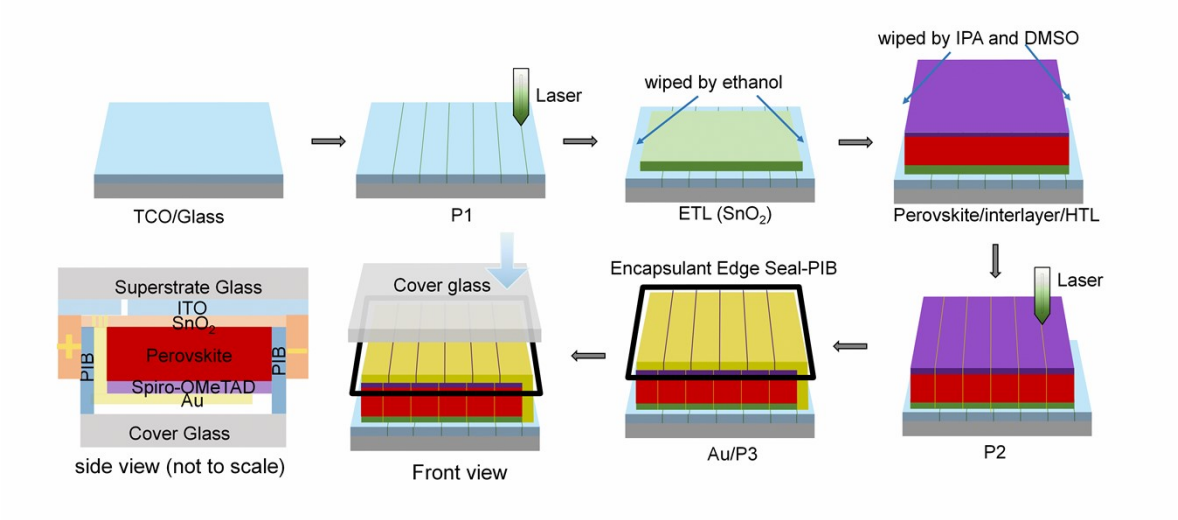

Fig. S15 Illustrations of the encapsulation process of PSMS (not to scale).

Supplementary References:

1. L. Shi, M. P. Bucknall, T. L. Young, M. Zhang, L. Hu, J. Bing, D. S. Lee, J. Kim, T. Wu, N. Takamura, D. R. McKenzie, S. Huang, M. A. Green and A. W. Y. Ho-Baillie, *science*, 2020, **368**, eaba2412.
2. Y. Deng, S. Xu, S. Chen, X. Xiao, J. Zhao, J. Huang, *Nat. Energy*, 2021, 2021, **6**, 633-641.
3. Y. Sha, E. Bi, Y. Zhang, P. Ru, W. Kong, P. Zhang, X. Yang, H. Chen and L. Han, *Adv. Energy Mater.,* 2021, **11**, 2003301.
4. Z. Yang, W. Zhang, S. Wu, H. Zhu, Z. Liu, Z. Liu, Z. Jiang, R. Chen, J. Zhou, Q. Lu, Z. Xiao, L. Shi, H. Chen, L. K. Ono, S. Zhang, Y. Zhang, Y. Qi, L. Han and W. Chen, *Sci. Adv.,* 2021, **7**, eabg3749.
5. A. Ren, H. Lai, X. Hao, Z. Tang, H. Xu, B. M. F. Yu Jeco, K. Watanabe, L. Wu, J. Zhang, M. Sugiyama, J. Wu and D. Zhao, *Joule,* 2020, **4**, 1263-1277.
6. E. Bi, W. Tang, H. Chen, Y. Wang, J. Barbaud, T. Wu, W. Kong, P. Tu, H. Zhu, X. Zeng, J. He, S.-i. Kan, X. Yang, M. Grätzel and L. Han, *Joule,* 2019, **3**, 2748-2760.
7. Z. Liu, L. Qiu, L. K. Ono, S. He, Z. Hu, M. Jiang, G. Tong, Z. Wu, Y. Jiang, D.-Y. Son, Y. Dang, S. Kazaoui and Y. Qi, *Nat. Energy,* 2020, **5**, 596-604.
8. H. Chen, F. Ye, W. Tang, J. He, M. Yin, Y. Wang, F. Xie, E. Bi, X. Yang, M. Grätzel and L. Han, *Nature,* 2017, **550**, 92-95.
9. K. Zhao, L. Zhang, R. Xia, Y. Dong, W. Xu, C. Niu, L. He, M. Yan, L. Qu, L. Mai, *Small* 2016, **12**, 588-594.
10. X. Zhang, Z. Jin, J. Zhang, D. Bai, H. Bian, K. Wang, J. Sun, Q. Wang and S. F. Liu, *ACS Applied Materials & Interfaces,* 2018, **10**, 7145-7154.
11. C. Tian, A. Mei, S. Zhang, H. Tian, S. Liu, F. Qin, Y. Xiong, Y. Rong, Y. Hu, Y. Zhou, S. Xie, H. Han, *Nano Energy* 2018, **53**, 160-167.
12. C. Tian, S. Zhang, A. Mei, Y. Rong, Y. Hu, K. Du, M. Duan, Y. Sheng, P. Jiang, G. Xu, H. Han, ACS *Appl. Mater. Interfaces,* 2018, **10**, 10835-10841.
13. J. Du, J. Duan, Q. Guo, Y. Duan, X. Yang, Q. Zhou and Q. Tang, *J. Mater. Chem. A*, 2021, DOI: 10.1039/D1TA07090H.